INTERNATIONAL JOURNAL OF HYDROGEN ENERGY XXX (2018) 1–12

Available online at www.sciencedirect.com

ScienceDirect

journal homepage: www.elsevier.com/locate/he

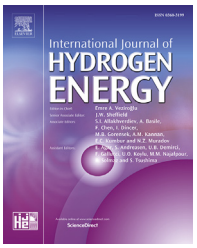

Cermets Ni/($Ce_{0.9}Ln_{0.1}O_{1.95}$) (Ln = Gd, La, Nd and Sm) prepared by solution combustion method as catalysts for hydrogen production by partial oxidation of methane

Consuelo Alvarez-Galvan [a,*], *Horacio Falcon* [b], *Vanessa Cascos* [c], *Loreto Troncoso* [c], *Susana Perez-Ferreras* [a], *Maricarmen Capel-Sanchez* [a], *Jose M. Campos-Martin* [a], *Jose Antonio Alonso* [c], *Jose L.G. Fierro* [a]

[a] *Instituto de Catálisis y Petroleoquímica, CSIC, Cantoblanco, E-28049, Madrid, Spain*
[b] *Centro de Investigación y Tecnología Química (CITeQ), Universidad Tecnológica Nacional-Facultad Regional Córdoba, X5016ZAA, Córdoba, Argentina*
[c] *Instituto de Ciencia de Materiales de Madrid, CSIC, Cantoblanco, E-28049, Madrid, Spain*

ARTICLE INFO

Article history:
Received 31 August 2017
Received in revised form
3 April 2018
Accepted 4 April 2018
Available online xxx

Keywords:
Cermets
SCS
Methane
Partial oxidation
Hydrogen

ABSTRACT

Catalysts based on Ni/($Ce_{0.9}Ln_{0.1}O_{1.95}$) (Ln = Gd, La, Nd and Sm) have been developed and tested for hydrogen production by partial oxidation of methane. The synthesis method (SCS, solution combustion synthesis) produces macroporous composite materials composed of ceramic (cer, $Ce_{0.9}Ln_{0.1}O_{1.95}$) and metallic (met, Ni) phases, without the need of an activation stage prior to the catalytic reaction. The catalysts have been characterized by different techniques: X-ray diffraction, N_2 adsorption-desorption, Hg porosimetry, Scanning Electron Microscopy, Temperature Programmed Reduction, H_2 and O_2 pulse chemisorption, X-ray photoelectron spectroscopy and Raman spectroscopy. With the exception of the lanthanum-loaded catalyst, the catalysts are highly active, selective and stable; being the one doped with gadolinium the most efficient. Correlations structure-activity point out that the excellent catalytic performance is related to the high catalytic surface area per unit mass of catalyst and to an appropriate balance of nickel dispersion to oxygen vacancies of the support.

Introduction

There is a great economic incentive in developing efficient catalysts for the conversion of natural gas into valuable products. Natural gas is found in many locations around the world (more distributed than oil reserves) and avoids dependence from oil producer countries; however the main drawback to use methane as a source of chemicals and fuels is the relatively low cost of oil coupled with the high cost of natural gas storage and transportation from remote reservoirs. So far, the only economically available route for the conversion of methane into more valuable chemicals is via syngas production [1].

* *Corresponding author.*
E-mail address: c.alvarez@icp.csic.es (C. Alvarez-Galvan).

https://doi.org/10.1016/j.ijhydene.2018.04.025
0360-3199/

Thus, there is a great motivation in developing efficient catalysts for the conversion of natural gas into syngas (suitable for methanol and Fischer-Tropsch syntheses) or for hydrogen production. Among the existing technologies employed to reform natural gas: steam reforming (SRM), dry reforming (DRM) and partial oxidation of methane (POM), the POM reaction presents some advantages compared to the conventionally used, highly endothermic, methane steam reforming such as energy saving, since it is a mild exothermic reaction and leads to a H_2/CO ratio ~ 2 (suitable for Fischer-Tropsch or methanol syntheses). The thermodynamics indicates that methane conversion and selectivity to syngas is enhanced at high temperature, being necessary the use of a catalyst with thermal stability at high temperatures (around 700–800 °C). Their main problems are the formation of hot-spots in the catalytic bed and, in some cases, the need of an oxygen separation plant [2].

Supported Ni catalysts were found to be active for the former process, but suffer from deactivation caused by coke formation as well as sintering of Ni particles. In comparison, noble metal catalysts exhibit higher activity and stability; however, they are much more expensive and less readily available.

On the other hand, the support has also a role in the catalyst efficiency, changing the adsorption and reactivity of reactant molecules, decreasing carbon formation by their basicity or by the formation of carbonates, containing oxygen vacancies and enhancing oxygen mobility and tuning the dispersion of the supported active phase by the different interaction with the support. The use of rare earths as supports results in efficient catalysts for oxidation reactions, increases the oxygen storage/release capacity oxidizing deposited carbon and produces a strong interaction with active phase, decreasing sintering [3–7].

Considering the advantages of both metal and support phases, Ni-ceria supported catalysts have been successfully used as catalysts for catalytic partial oxidation of methane (CPOM). It was found that oxygen mobility in the support is enhanced by metal-support interaction, which is influenced by the preparation method [8]. The influence of the amount of nickel on catalytic performance has been also investigated [9] and, very importantly, the effect of Zr incorporation in the ceria lattice on the redox properties was identified, finding that the catalytic behavior is related to the metal dispersion and the surface oxygen mobility, promoting carbon elimination [10–14].

Although there is not a general consensus on the reaction mechanism, for a medium-high space velocity reaction, it is assumed that the reaction would proceed in two-stages: the first includes a combustion reaction and the second involves reforming reactions leading to CO_2 and H_2O, being necessary to favor heat transfer in order to facilitate these last endothermic reactions. The supported metallic phase would act by dissociating methane, followed by reaction with oxygen species from the support (in a Mars van Krevelen mechanism) to form syngas. Supported active particles with a higher oxidation state would facilitate a deeper oxidation [15].

Among various methods employed for catalysts preparation, solution combustion synthesis (SCS) is well suited for the synthesis of metal oxides of homogeneous, porous and finely particulate compositions. These are critical points in these materials, helping to improve heat and mass transfer and to decrease the formation of hot-spots [16,17].

Inspired by the latest developments in ceria-supported Ni catalysts [9,18,19], we focused on the preparation by the SCS method of nickel supported on mixed cerium oxides, doped with different lanthanides (Gd, La, Nd and Sm), in order to analyze the formation of oxygen vacancies and oxygen mobility, which would have an influence on oxygen adsorption and carbon gasification and their possible role in POM reaction.

Experimental

Preparation method

In this study, cermets $(Ni)_{0.1}(Ce_{0.9}Ln_{0.1}O_{1.95})_{0.9}$ (Ln = Gd, La, Nd and Sm) (coded NCG, NCL, NCN and NCS) were prepared by the SCS method. In a typical procedure, stoichiometric amounts of the corresponding nitrates are dissolved in distilled water, and then a certain amount of glycine is added [20]. The mixture is heated on a hot plate up to 310 °C. Upon the evaporation of water, a viscous gel is produced. Then a self-igniting or autocombustion process is produced, leading, in a single step, to a finely particulate powder consisting of nickel metal particles supported on the corresponding doped-ceria mixed oxide [17].

Characterization

The phase identification was performed by X-ray diffraction (XRD) analysis using a X'Pert Pro PANalytical equipment. XRD patterns were recorded using a CuKα radiation (λ = 1.5406 Å, 45 kV, 40 mA). The mean particle size was then estimated from X-ray line broadening using the Scherrer equation. Width was taken as the full width at half maximum intensity of the most intense and least overlapped peak of the doped-ceria support (2θ = 28.4°). XRD data were analyzed by the Rietveld method [21] with the FULLPROF program [22]. A pseudo-Voigt function was chosen to generate the line shape of the diffraction peaks. The following parameters were refined in the final run: scale factor, background coefficients, zero-point error, pseudo-Voigt corrected for asymmetry parameters, positional coordinates and isotropic thermal factors for all the atoms.

Specific surface areas were calculated using the BET method from the nitrogen adsorption isotherms recorded at 196 °C using a Micromeritics ASAP 2420 automatic instrument. The total pore volume, total pore area and pore size distribution were determined using mercury porosimetry (Micromeritics AutoPore IV 9510).

Temperature-programmed reduction (TPR) experiments were carried out in an automatic Micromeritics TPD/TPR 2900. The catalyst was pretreated under helium at 110 °C for 15 min. The TPR profile was recorded by heating the sample from room temperature to 800 °C at a rate of 10 °C min^{-1} under a H_2/Ar (10% v/v) flow.

Metallic nickel surface area of the catalysts and the amount of chemisorbed oxygen for the supports were

Please cite this article in press as: Alvarez-Galvan C, et al., Cermets Ni/$(Ce_{0.9}Ln_{0.1}O_{1.95})$ (Ln = Gd, La, Nd and Sm) prepared by solution combustion method as catalysts for hydrogen production by partial oxidation of methane, International Journal of Hydrogen Energy (2018), https://doi.org/10.1016/j.ijhydene.2018.04.025

determined by pulse chemisorption, with H_2 and O_2, respectively, using a Micromeritics Autochem II 2920 equipment. Prior to any chemisorption measurements, the samples were pretreated at 700 °C (15 °C min^{-1}) first in helium for 15 min, and then in H_2 (10%)/Ar at 350 °C for 10 min to reduce surface nickel oxide particles completely. Then, for H_2 pulse chemisorption: (i) H_2 was flushed increasing the temperature to 375 °C in helium (15 °C min^{-1}) for 10 min (ii) the temperature was decreased in argon flow up to 25 °C (iii) the metallic surface area was evaluated by pulse chemisorption technique, applying measured doses of hydrogen until no change in the hydrogen peak is observed, assuming a stoichiometry of one hydrogen atom per surface nickel atom. For O_2 pulse chemisorption: (i) the temperature was increased in helium flow up to 700 °C (15 °C min^{-1}) for 10 min (ii) then oxygen pulses were applied, until no change in the oxygen peak is observed [23].

The morphology of the catalysts at the micrometer level was studied by Scanning Electron Microscopy (SEM) using a Hitachi TM-1000 with an acceleration voltage of 15 kV.

The morphology of the catalysts (at nanometer scale resolution) was studied by High Resolution Transmission Electron Microscopy (HRTEM). The images of the fresh catalysts were recorded on a JEOL JEM-3010 transmission electron microscope (300 kV). The preparation method consisted of dropping a suspension of the sample in isopropanol on a copper grid covered by a carbon film.

XPS measurements were recorded using a Escalab 200R spectrometer equipped with a hemispherical electron analyzer and an Al Kα ($h \cdot \nu = 1486.6$ eV) 120 W X-ray source. The area of the peaks was estimated by calculating the integral of each peak after smoothing and subtraction of a S-shaped background and fitting of the experimental curve to a mixture of Lorentzian and Gaussian lines (90G/10L). All binding energies (BE) were referenced to the C 1s signal at 284.8 eV from carbon contamination of the samples to correct the charging effects. Quantification of the atomic fractions on the sample surface was obtained by integration of the peaks normalized with atomic sensitivity factors.

Raman spectra were recorded with a Renishaw in Via Raman Microscope spectrometer equipped with a laser beam emitting at 785/532 nm, at 300/100 mW output power. The photons scattered by the sample were dispersed by a 1800/1200 lines/mm grating monochromator and simultaneously collected on a CCD camera; the collection optic was set at 50 × objective.

Catalytic activity tests

The catalytic behavior of the catalysts obtained by SCS (NCG, NCL, NCN and NCS) as well as of the support (CG, $Ce_{0.9}Gd_{0.1}O_{1.95}$) for the partial oxidation of methane to syngas was studied under atmospheric pressure, at 700 °C using a quartz fixed bed reactor (external diameter = 6 mm, internal diameter = 4 mm). The catalysts (40 mg) were subjected to a pretreatment under N_2 flow at 700 °C for 1 h, prior to the reaction. The space velocity was 36600 $mL_N\ h^{-1}\ g^{-1}$ and the feed composition was 40% CH_4, 20% O_2 and 40% N_2 (molar). The reaction stream was analyzed on line by gas chromatography (HP 6890), equipped with a column Carboxen 1010 PLOT (SUPELCO®) and with a thermal conductivity detector. This system was used to analyze H_2, O_2, N_2, CO, CO_2 and CH_4. Nitrogen was used as an inert standard for quantification.

Results and discussion

Crystalline phases

The XRD patterns of samples $(Ni)_{0.1}(Ce_{0.9}Ln_{0.1}O_{1.95})_{0.9}$ (Ln = Gd, La, Nd and Sm) (Fig. 1a) show intense and sharp diffraction lines at angles 2θ of 28.6°, 33.1°, 47.4° and 56.4° corresponding to the reflection planes (111), (200), (220) and (311) of fluorite-structured $Ce_{0.9}Ln_{0.1}O_{1.95}$.

Diffraction lines corresponding to metallic nickel cannot be distinguished. Other results obtained by our research group showed that these diffraction lines could only be observed for

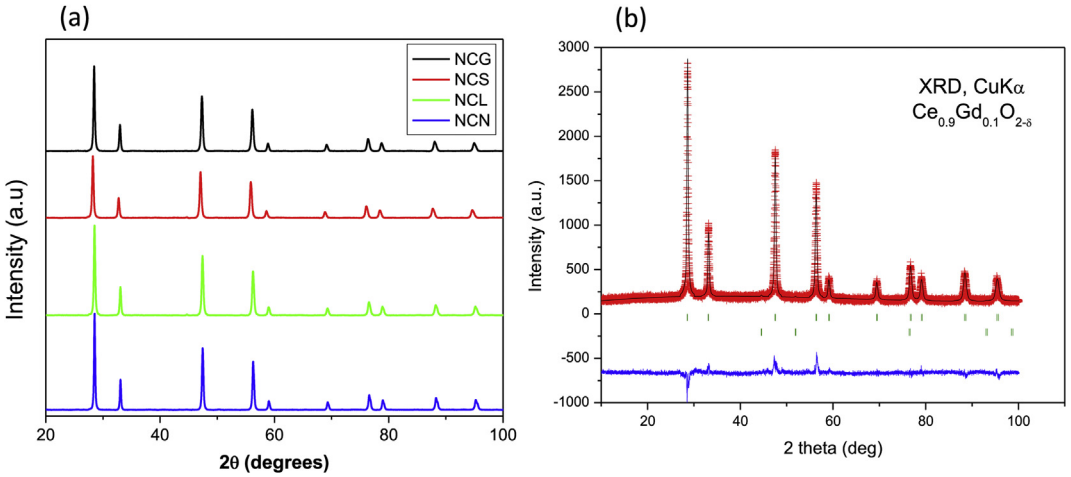

Fig. 1 – (a) X-ray diffraction profiles for the catalysts NCG, NCL, NCN and NCS. (b) Observed (crosses), calculated (full line) and difference (at the bottom) XRD profiles for $Ce_{0.9}Gd_{0.1}O_{2-\delta}$ at 298 K, refined in the cubic Fm-3m space group. The two series of vertical markers correspond to the allowed Bragg reflections for the fluorite and Ni metal, respectively.

Please cite this article in press as: Alvarez-Galvan C, et al., Cermets Ni/($Ce_{0.9}Ln_{0.1}O_{1.95}$) (Ln = Gd, La, Nd and Sm) prepared by solution combustion method as catalysts for hydrogen production by partial oxidation of methane, International Journal of Hydrogen Energy (2018), https://doi.org/10.1016/j.ijhydene.2018.04.025

nickel loadings of 0.5 M and above. However, for the catalysts studied in this work (molar amount of nickel = 0.1, per mol of cermet) the color and ferromagnetic character of the samples revealed the metallic state of nickel right after being prepared by SCS method.

Rietveld refinement allowed to confirm that the unit cell parameter decreases with the decrease in the ionic radius of the lanthanide, indicating the inclusion of the respective lanthanide cation into the ceria lattice (Fig. 2) [24].

A XRD study at room temperature (RT) for $Ce_{0.9}Ln_{0.1}O_{2-\delta}$ (Ln = La, Nd, Sm, Gd) was useful to investigate the structural details. The crystal structure of the fluorite phase was defined in the cubic Fd-3m (No 225) space group, Z = 4. Ce and Ln atoms are distributed at random at 4*a* (0,0,0), and oxygen atoms O at 8*c* (1/4,1/4,1/4) sites. The occupancy factors of oxygen atoms were also refined in the final run. The weak scattering of O with respect to heavy atoms such as Ce and Ln did not allow detecting the subtle sub-stoichiometry of the oxygen lattice; the occupancy factors of O converged at 2.02 (1) per formula. The cermet is a composite of fluorite and metal Ni. This metal was also included in the refinement as a second phase, also defined in the Fm-3m space group, with Ni at 4a sites (0,0,0) and unit-cell parameter **a** = 3.522 Å. Given the relatively small amount of Ni (3.6% in weight in this cermet family) and the high metal dispersion achieved by SCS catalysts preparation method, is hardly visible in the XRD diagram. The structural view inserted in Fig. 2 displays the fluorite structure, where Ce and Ln ions are coordinated to 8 oxygen atoms at equal distances in cubic coordination. Fig. 1b illustrates the good agreement between the observed and calculated XRD patterns for $Ce_{0.9}Gd_{0.1}O_{2-\delta}$ at room temperature; similar plots are obtained for R = La, Nd and Sm. The second series of Bragg reflections correspond to Ni metal, which is hardly visible in the XRD profiles. Table 1 summarizes the unit-cell, atomic, thermal parameters and discrepancy factors after the Rietveld refinement of $Ce_{0.9}Gd_{0.1}O_{2-\delta}$ at room temperature. The unit cell parameters for $Ce_{0.9}Ln_{0.1}O_{2-\delta}$ (Ln = La, Nd, Sm, Gd) are **a** = 5.4333(2), 5.5275(2), 5.4178(2) and 5.4134 (2) Å, respectively; they progressively decrease along the series as corresponds to the lanthanide contraction of the doping Ln^{3+} ion.

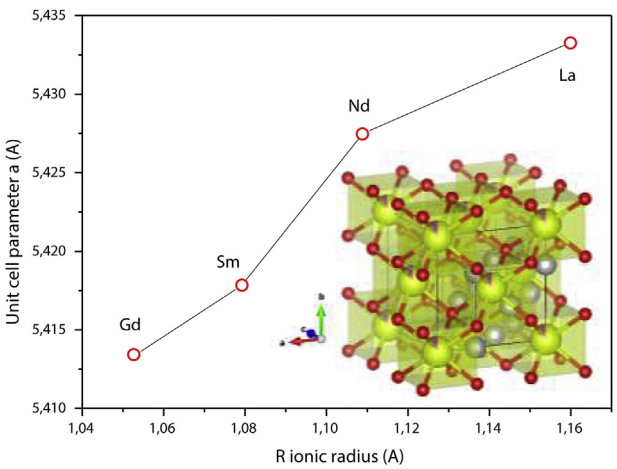

Fig. 2 – Unit cell parameter versus lanthanide ionic radius for the catalysts NCG, NCL, NCN and NCS and fluorite structure for $Ce_{0.9}Gd_{0.1}O_{2-\delta}$ (inserted figure).

Table 1 – Atomic parameters, interatomic distances and angles for $Ce_{0.9}Gd_{0.1}O_{2-\delta}$ in the cubic Fm-3m (N^0 225) space group, Z = 4, from XRD data at 298 K a = 5.4134 (2) Å. Discrepancy factors: Rp = 6.31%, Rwp = 7.95%, Rexp = 6.79%, RBragg = 10.15%.

	Wyckoff site	x	y	z	U_{iso}	Occ. (<1)
Ce	4*a*	0.00000	0.00000	0.00000	0.3	0.90000
Gd	4a	0.00000	0.00000	0.00000	0.3	0.10000
O	8c	0.25000	0.25000	0.25000	0.7	1.020 (11)

The average domain size of the catalyst support (constituted of lanthanide-doped ceria), was calculated by the Scherrer equation. The results, reported in Table 2, show similar crystallites sizes, being found the following trend: NCG < NCS < NCL < NCN. According to Kullgren et al. [25], the smaller size of the crystallites would involve a greater proportion of oxygen vacancies.

Textural properties

Pore size distributions obtained by Hg intrusion porosimetry are depicted in Fig. 3. Obtained profiles essentially correspond to macroporous solids with a pore size distribution in the range of 0.1–100 μm. As reported in Table 2, the total surface areas, determined by this technique, are between 8.6 and 10.4 $m^2\ g^{-1}$. The porosity of these catalysts is very high, having found values between 84 and 95%. The lanthanum-doped sample presents the lowest porosity while the others exhibit values above 92%. The average pore diameter is around 2 μm for the catalyst NCG; for NCN and NCS it is close to 3 μm, while for the lanthanum-doped sample (NCL), it is around 1 μm. For all the samples, a relative maximum for pore diameter around 1.2–1.4 μm is observed. The shift produced in the profile for a pore diameter around 6 μm, especially in the sample doped with Nd, is considered an artifact due to the change from low to high pressure during the porosimetry analysis. The BET surface areas of the catalysts have been also determined by N_2 adsorption-desorption at −196 °C and the values, which are reported in Table 2, are between 9 and 15 $m^2\ g^{-1}$.

Morphology

The morphology of the catalysts was studied by SEM and TEM. Fig. 4 shows SEM images at ×2.5 magnification. The micrographs show a foam-like morphology, with highly macroporous texture, characteristic of SCS-prepared solids [26]. The average pore size is in the order of that determined by Hg porosimetry, between 1 and 3 μm. At this magnification, the foam-like microstructure is more noticeable for the catalyst NCG. For the catalyst NCL, the morphology is somewhat different, since the formation of microprotuberances in the form of microflowers are observed.

Fig. 5 shows representative HRTEM pictures of NCG catalyst, by way of example. The picture obtained at lower magnification allows the observation of the great macroporosity. The crystalline lattice of a representative ceria crystallite is marked with a circle around it. In this case, it

Please cite this article in press as: Alvarez-Galvan C, et al., Cermets Ni/($Ce_{0.9}Ln_{0.1}O_{1.95}$) (Ln = Gd, La, Nd and Sm) prepared by solution combustion method as catalysts for hydrogen production by partial oxidation of methane, International Journal of Hydrogen Energy (2018), https://doi.org/10.1016/j.ijhydene.2018.04.025

Table 2 – Physicochemical properties for fresh catalysts.

Catalysts	Textural properties				Average crystalline domain (nm)	Chemisorbed O_2 (cm^3/g) for supports	Chemisorbed H_2 (cm^3/g) for catalysts
	A_{BET} (m^2/g)	Total pore area (m^2/g)	Porosity (%)	Average pore diameter (μm)			
NCG	8.8.8	8.6	92.4	2.03	25.7	0,380	0059
NCL	14.4	8.9	84.1	0.91	29.3	0,388	0090
NCN	10.8	10.4	95.3	2.96	30.0	1031	0,192
NCS	12.5	9.4	94.3	2.87	28.9	0,705	0148

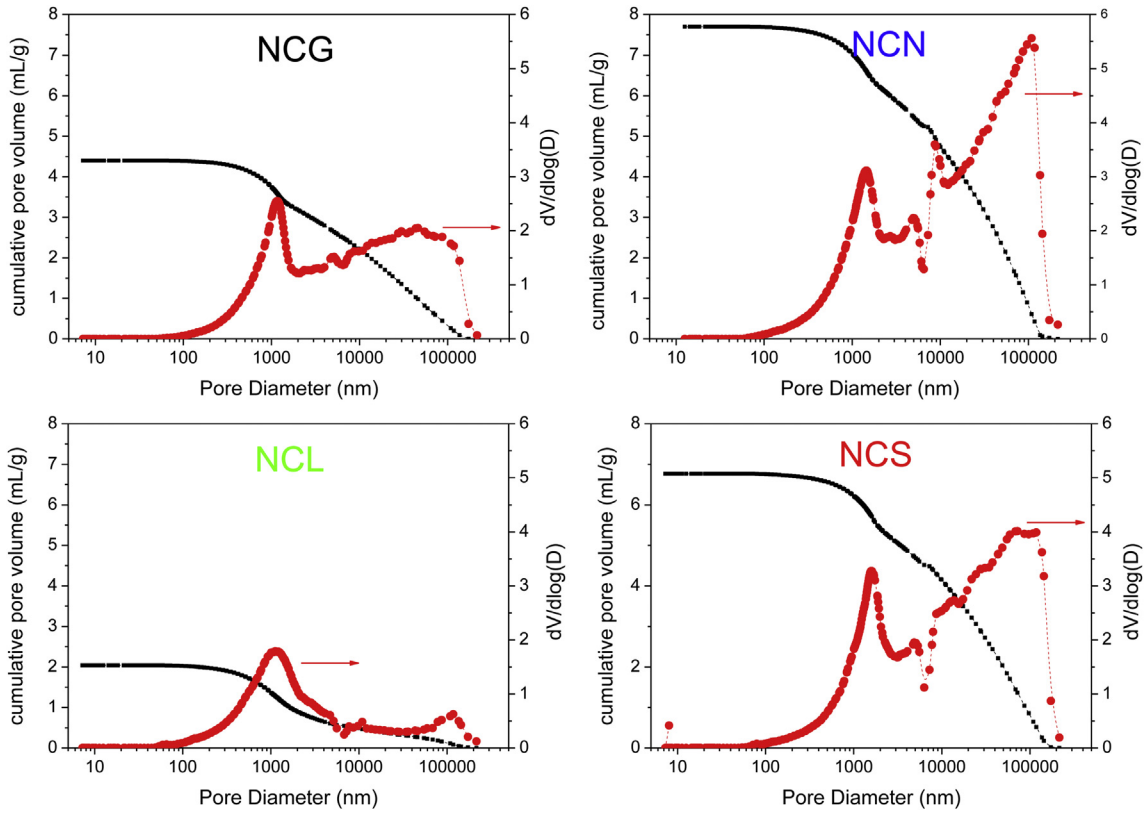

Fig. 3 – Pore size distribution profiles (by Hg intrusion porosimetry) for the catalysts NCG, NCL, NCN and NCS.

corresponds to the crystal plane spaces of CeO_2 (111). The detection of nickel particles is not easy, since its size is quite small (domain size lower than 2 nm, as derived from XRD results) and the contrast with the support is not high, making it difficult to distinguish them.

Reducibility and nickel surface area in catalysts, and chemisorbed oxygen in supports

Both supported metallic nickel particles and support have a role in the CPOM reaction. Thus, methane adsorbed on the Ni surface is dissociated to form hydrogen and carbon. This carbon, when is close to the interface metal-support, is oxidized to carbon monoxide with oxygen from the support. Then, formed oxygen vacancies are replenished by gaseous oxygen. Metal particles also accelerate the oxygen exchange with the support, promoting oxygen spillover from the metal to the support. The lattice oxygen also removes the carbon adsorbed on metallic nickel particles. The replacement of cerium ions in ceria by lanthanide cations results in the formation of a defective fluorite structured solid solution, incorporating oxygen vacancies distributed at random in the crystal structure. This modification of the ceria lattice increases the oxygen storage capacity and the dispersion of metals supported on the doped ceria [27,28].

Catalysts reducibility was determined by Temperature Programmed Reduction, with the aim to evaluate the oxygen transfer capacity. From reduction profiles (Fig. 6) it is clear that the samples show defined hydrogen consumptions between 200 and 300 °C, which are attributed to the reduction of small surface particles of NiO weakly interacting with the support. Above 400 °C, hydrogen consumption is attributed to the reduction of high-dispersed non-crystalline NiO species, while peaks with reduction temperatures between 500 and 650 °C are related to the reduction of species in intimate contact with CeO_2 [29]. Above 630 °C, a wide consumption is assigned to the reduction of the ceria phase [30]. The hydrogen consumption related to the support started at a similar

Please cite this article in press as: Alvarez-Galvan C, et al., Cermets Ni/($Ce_{0.9}Ln_{0.1}O_{1.95}$) (Ln = Gd, La, Nd and Sm) prepared by solution combustion method as catalysts for hydrogen production by partial oxidation of methane, International Journal of Hydrogen Energy (2018), https://doi.org/10.1016/j.ijhydene.2018.04.025

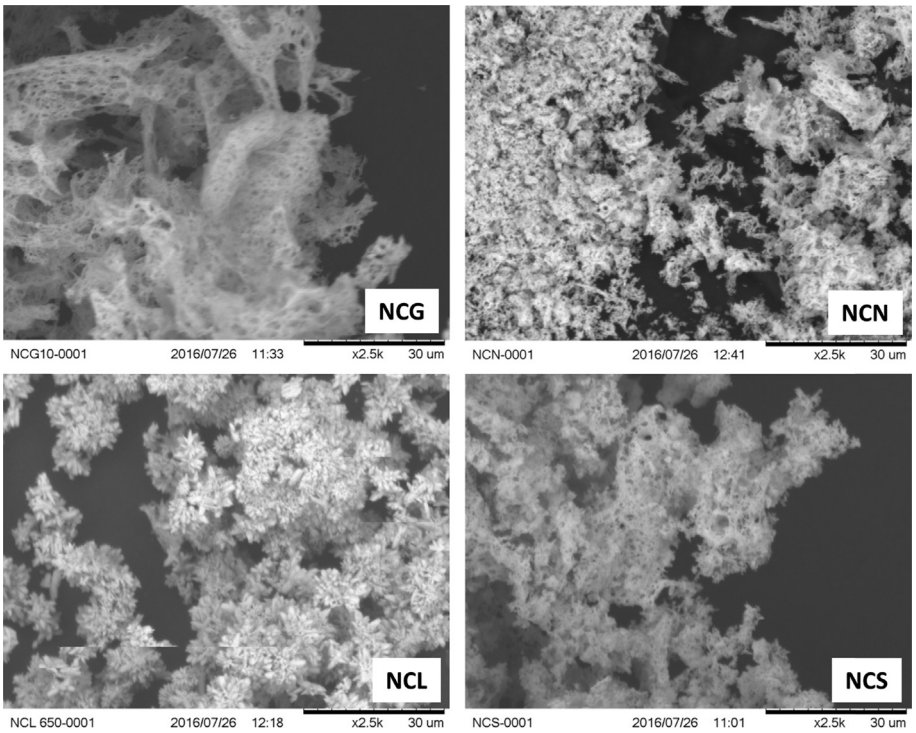

Fig. 4 – Scanning Electron Microscopy (SEM) micrographs for the catalysts NCG, NCL, NCN and NCS.

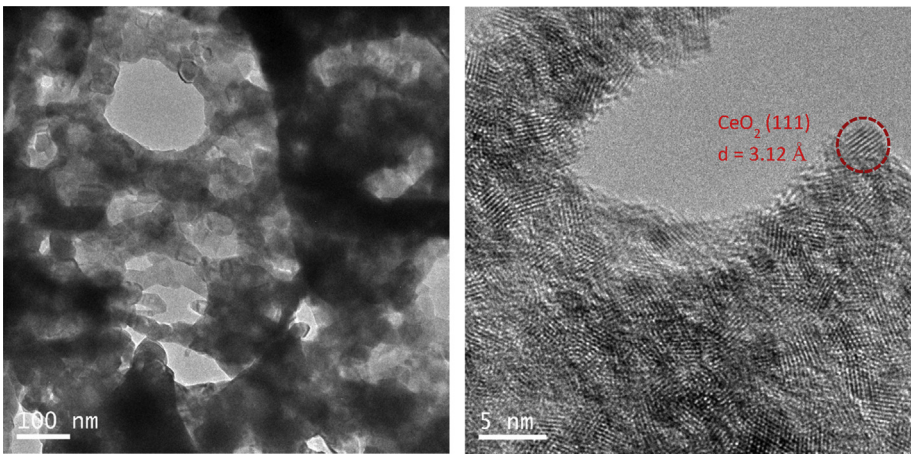

Fig. 5 – Transmission Electron Microscopy (TEM) micrographs for the catalyst NCG.

temperature and was too wide to establish any correlation with the oxygen transfer capacity.

Although we found by XRD that bulk nickel was in the metallic state, the contact of this phase with atmospheric air produces a surface oxidation of nickel; that is, the particles have a core formed by metallic nickel and there is also a thin external layer composed of NiO. This is why a small H_2 consumption is observed by TPR analyses. This observation has been derived from the quantification of hydrogen consumption for each profile (data reported in Table 3). The reduction of nickel species in intimate contact with ceria and the reduction of ceria are overlapped and these contributions are not large in comparison with the other hydrogen consumptions. Because of this, in order to calculate the proportion of nickel that is oxidized, we have assumed that all the area under the curve corresponds to the reduction of nickel oxide species to metallic nickel.

Concerning surface Ni^0 area (obtained from H_2 pulse chemisorption), depicted in Table 2, the following order is found: NCN > NCS > NCL > NCG. On the other hand, in an attempt to quantify the oxygen storage capacity, the amount of chemisorbed oxygen of the supports at the reaction temperature was revealed by O_2 pulse chemisorption, being found the following trend: CeNd > CeSm > CeLa ~ CeGd.

As previously commented, surface lattice oxygen was found to selectively oxidize methane to form carbon

Please cite this article in press as: Alvarez-Galvan C, et al., Cermets Ni/($Ce_{0.9}Ln_{0.1}O_{1.95}$) (Ln = Gd, La, Nd and Sm) prepared by solution combustion method as catalysts for hydrogen production by partial oxidation of methane, International Journal of Hydrogen Energy (2018), https://doi.org/10.1016/j.ijhydene.2018.04.025

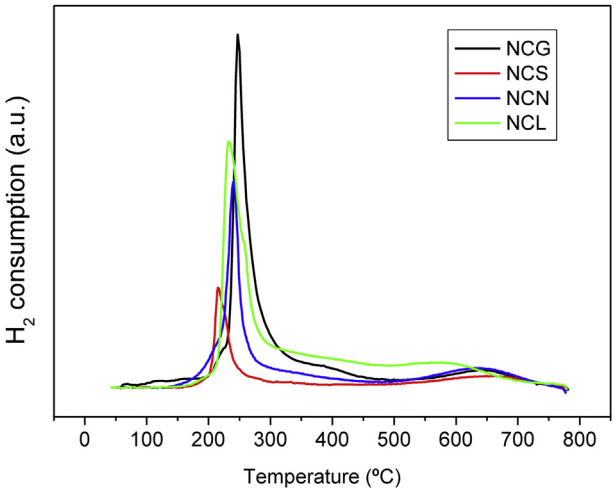

Fig. 6 – Temperature Programmed Reduction profiles for the catalysts NCG, NCL, NCN and NCS.

monoxide and hydrogen. The amount of chemisorbed oxygen would be related to the oxygen storage capacity and also to the decrease in the formation of carbon, during syngas formation, since the high oxygen mobility, promoted by lanthanide doping of ceria, was reported to accelerate surface carbon oxidation reactions, inhibiting carbon growth [28,31]. However, although both Ni surface area (related to chemisorbed H_2) and chemisorbed O_2 have role in the reaction, as we will see later on in the "Structure-activity correlations section", the performance of the catalyst is influenced by a proper balance between the oxygen storage capacity of the support and metal dispersion [27,28].

Chemical surface analysis in spent catalysts

XPS was used to determine the chemical state of the elements and their surface proportions in the catalysts after reaction. For each sample, Ce 3d, Ln 3d (Ln: Gd, La, Nd, Sm), Ni 2p, O 1s and C 1s core level spectra were recorded and the respective binding energies for above levels are reported in Table 4. Binding energies for Ni $2p_{3/2}$ core level are in the range 855.3–855.5 eV. These values together with its strong satellite line that appears around 861–862 eV confirm the presence of Ni^{2+} species on the surface of the catalysts after reaction.

By way of example, XPS spectra of Ni 2p core-level for a representative catalyst (NCG, before and after reaction) are depicted in Fig. 7. These profiles present a satellite peak around 861.8 eV which is the footprint of Ni^{2+}. Moreover, the ratio between the area corresponding to the satellite line and the area of the main line of Ni 2p3/2 are similar for both samples, the catalyst before and after reaction.

Table 4 – Binding energies (eV) of core electrons of NCLn (Ln = Gd, La, Nd and Sm) for spent catalysts.

Catalysts	Ce3d	Ln3d	Ni2p	O1s	C1s
NCL us	882.2	834.8	855.4	529.3 (64) 531.7 (36)	288.5
NCS us	882.4	1081.2	855.5	529.2 (61) 531.5 (39)	288.3
NCG us	882.2	140.9	855.5	529.2 (60) 531.6 (40)	288.6
NCN us	882.3	121.4	855.3	929.3 (59) 932.6 (41)	288.4

The XPS spectra of Ce 3d core-levels is formed by six peaks corresponding to four pairs of spin–orbit doublets, characteristic of oxidized Ce^{4+} species. The spectra profile and one of the satellite lines placed close to 917 eV, indicate that Ce^{4+} is the dominant surface ceria species for all the samples [32,33]. By evaluating the binding energy values of Gd (140.9 eV for $4d_{5/2}$), La (834.8 eV for $3d_{5/2}$), Nd (121.4 eV for $4d_{5/2}$) and Sm (1081.2 eV for $3d_{5/2}$) present in the catalysts after reaction, it can be concluded that these lanthanides are present in their 3 + oxidation state. Concerning the O 1s core level, the spectra show two different contributions, one centered at 529.2–529.3 eV, ascribed to oxygen species in the oxide lattice, and a second one, centered around 531.6 eV, which is assigned to oxygen present in adsorbed carbonates and/or hydroxyls groups. The relative proportions (lattice oxygen/adsorbed oxygen) species for the catalysts NCG and NCS are 60/40 and 61/39, respectively. For NCL is 64/36 and for the catalyst NCN is 59/41. On the other hand, C 1s spectra show two different bands, at 284.6 eV, assigned to adventitious carbon contamination (C–C and/or C–H species), and another, more intense, at 288.3–288.6 eV, assigned to C–O bonds in carbonates and coke precursors [34,35].

The atomic surface compositions (% at), calculated from XPS data, are reported in Table 5. Due to the partial overlapping of Ni $2p_{3/2}$ emission with La $3d_{3/2}$ emission, quantitative estimation of Ni proportion was done after careful deconvolution between both core-levels.

In order to compare the dispersion of the different active phases, the surface proportions of Ni, Ce and Ln (Gd, La, Nd, Sm) have been compared with the respective nominal compositions, excluding surface carbon and oxygen. As reported in Table 5, surface nickel proportion is somewhat lower than

Table 3 – Quantification of H_2 consumption (from H_2-TPR profiles).

Catalyst	Moles of H_2 consumed	Milimoles NiO	mg Ni	% Ni (weight)	% Ni (nominal)	Relative proportion of NiO respect to nominal Ni (%)
NCG	$5.53 \cdot 10^{-5}$	0.0553	3.240	0.0810	3.62	2.2
NCL	$5.69 \cdot 10^{-5}$	0.0569	3.339	0.0834	3.65	2.3
NCN	$3.16 \cdot 10^{-5}$	0.0316	1.855	0.0464	3.64	1.3
NCS	$1.34 \cdot 10^{-5}$	0.0134	0.786	0.0197	3.63	0.5

Please cite this article in press as: Alvarez-Galvan C, et al., Cermets Ni/($Ce_{0.9}Ln_{0.1}O_{1.95}$) (Ln = Gd, La, Nd and Sm) prepared by solution combustion method as catalysts for hydrogen production by partial oxidation of methane, International Journal of Hydrogen Energy (2018), https://doi.org/10.1016/j.ijhydene.2018.04.025

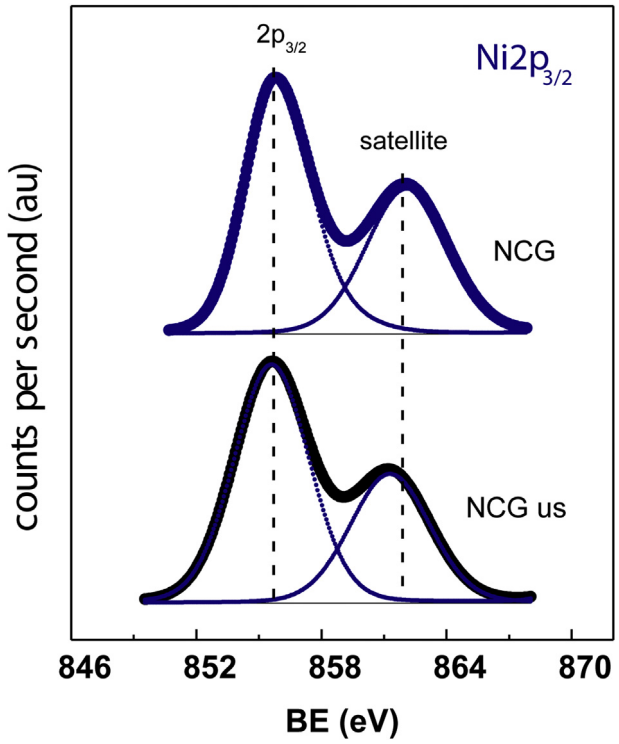

Fig. 7 – Ni 2p XPS spectra of fresh and spent NCG catalyst.

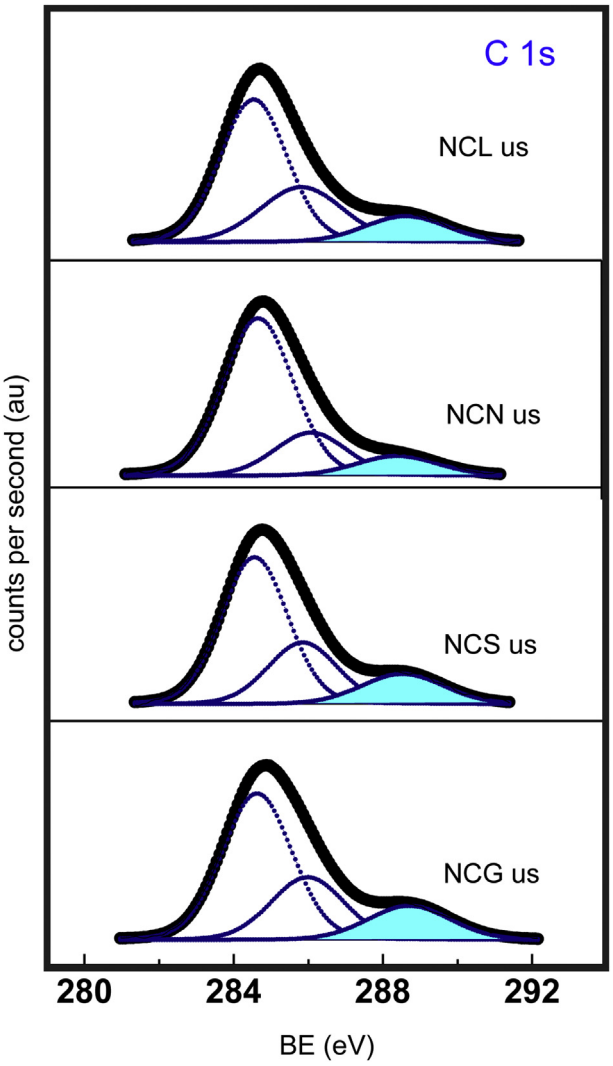

Fig. 8 – C 1s XPS spectra of the catalysts NCG, NCL, NCN and NCS after reaction.

nominal one (24.7%) but similar for all the catalysts after reaction, between 12.3% for NCS to 14.5% for NCL. Regarding the surface proportion of the lanthanides, used as dopants into ceria lattice, as derived from calculated values, they are between 3.2% for NCG to 5.1% for NCN, somewhat lower than the nominal one (10%).

Concerning surface carbon proportion, the surface-atom in % is between 6 and 8.4%, with the highest proportion corresponding to the catalyst doped with lanthanum. This highest carbon proportion could be associated with a larger carbon

Table 5 – Surface atomic proportions of Ce, Ln (Gd, La, Nd, Sm), Ni, O and C for spent catalysts.

Catalysts after reaction	Surface atomic % (XPS) in parenthesis (without considering surface carbon); in brackets (without considering surface carbon and oxygen)				
	Ce (% at)	Ln (% at)	Ni (% at)	O (% at)	C (% at)
NCG us	18.1	0.6	3.0	71.1	7.2
	(19.5) [83.4]	(0.7) [2.8]	(3.2) [13.8]	(76.6)	
NCL us	15.8	0.7	2.8	72.3	8.4
	(17.2) [81.9]	(0.8) [3.6]	(3.1) [14.5]	(78.9)	
NCN us	14.9	0.8	2.6	75.6	6.1
	(15.9) [81.4]	(0.9) [4.4]	(2.7) [14.2]	(80.5)	
NCS us	17.1	0.7	2.5	73.0	6.7
	(18.3) [84.3]	(0.8) [3.4]	(2.7) [12.3]	(78.2)	
	Nominal atomic %				
	27.45	3.06	10.00	59.49	–
	Nominal atomic % (without considering oxygen)				
	67.8	7.6	24.7	–	–

Please cite this article in press as: Alvarez-Galvan C, et al., Cermets Ni/($Ce_{0.9}Ln_{0.1}O_{1.95}$) (Ln = Gd, La, Nd and Sm) prepared by solution combustion method as catalysts for hydrogen production by partial oxidation of methane, International Journal of Hydrogen Energy (2018), https://doi.org/10.1016/j.ijhydene.2018.04.025

deposition and/or with a higher formation of surface carbonates, due to the higher basic character of this oxide.

XPS spectra corresponding to C1s core level for the catalysts after reaction are depicted in Fig. 8. The spectra are deconvoluted in three components: those found at lower binding energy (around 284.6 and 286 eV) are due to adventitious carbon contamination and the third one, around 288.8 eV, is attributed to surface carbonates and/or some carbon deposits.

Partial oxidation of methane

Fig. 9 shows the catalytic performance of $(Ni)_{0.1}(Ce_{0.9}B_{0.1}O_{1.95})_{0.9}$ (B = Sm, Nd, La and Gd) catalysts for the partial oxidation of methane to syngas after 6 h on stream. Methane conversions over the different catalysts and the support (CG, $Ce_{0.9}Gd_{0.1}O_{1.95}$) are presented in Fig. 9a. It is observed that the catalyst type has an effect on the conversion of methane. With the exception of the catalyst doped with lanthanum, which suffered a pronounced loss of activity and selectivity, the others present stable conversions along the reaction time. The trend found for methane conversion and hydrogen yield is: NCG > NCS > NCN > NCL (Fig. 9a and b).

It is also evident that nickel particles have a role as active phase in the partial oxidation of methane to syngas, since the sample CG, without supported nickel particles, is much less active for methane conversion and only selective to methane combustion (Fig. 9c). The catalyst doped with Gd showed the highest CH_4 conversion and H_2 yield along the whole reaction period, with values approaching the thermodynamic equilibrium [2].

Carbon deposited in spent catalysts

The characterization of the carbon deposits for the fresh and spent catalysts was carried out by Raman spectroscopy (Raman spectra are shown in Fig. 10). For each catalyst, at least three Raman spectra were recorded in different areas to assure the homogeneity of the composition. All the samples showed a band around 460 cm^{-1} band which is attributed to the symmetrical stretching mode (νs (Ce–O)) of the CeO_8 vibrational unit (triply degenerate F2g mode), since this is the oxygen environment of cerium atoms in the cubic fluorite lattice of ceria. The weak band present at ~600 cm^{-1} corresponds to a doubly degenerate LO mode of CeO_2 [36]. This band is observed in nanosized samples and was linked to oxygen vacancies in the CeO_2 lattice [37]. For the fresh catalysts, only these bands are observed (Fig. 10a). On the contrary, for the spent catalysts, besides these bands related to the ceria-based support, additional bands due to the presence of carbon are found (Fig. 10b). Thus, the Raman spectra of carbon exhibited two quite sharp modes, the G (graphitic) peak around 1580 cm^{-1} and the D (disordered) peak around 1350 cm^{-1}. It is also observed a shoulder around 1600 cm^{-1} related to disordered carbon species [30]. Since the Raman bands depend on the amount of sample and morphology, in order to compare the carbon deposited on the samples, the sum of the bands intensities at 1350 and 1580 cm^{-1}

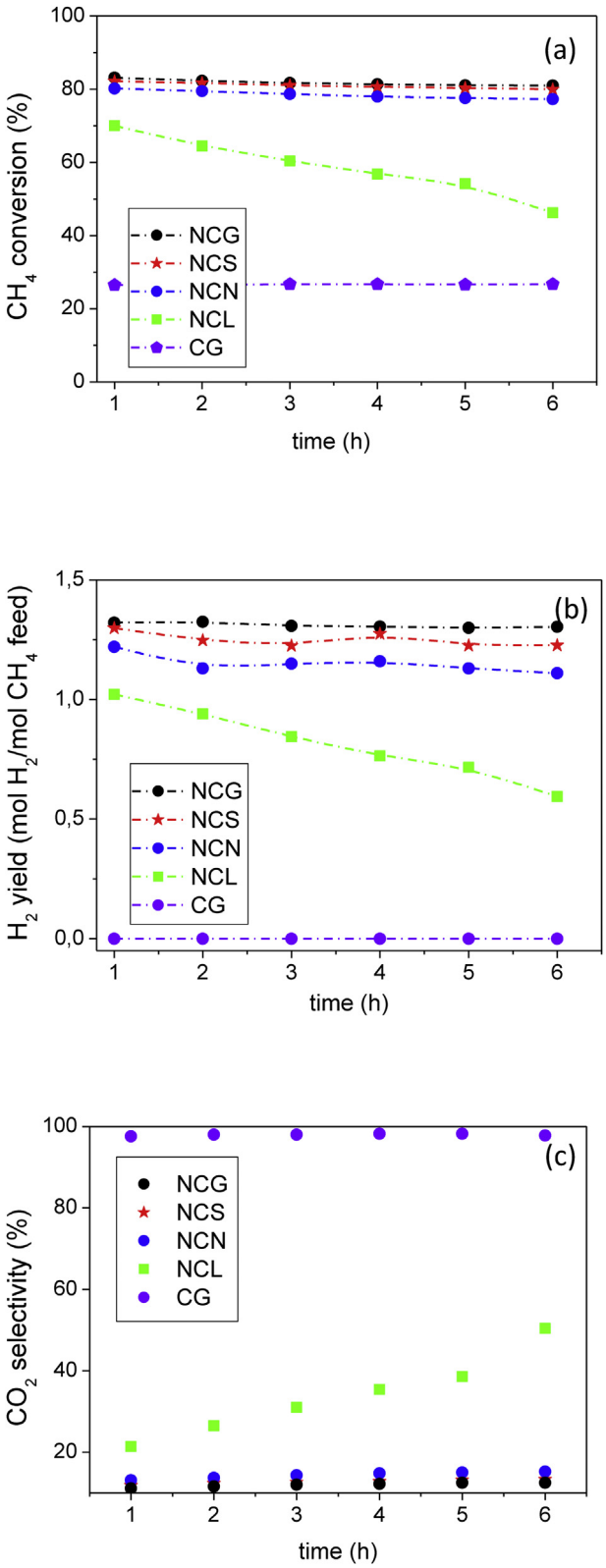

Fig. 9 – (a) CH_4 conversion (b) hydrogen yield (c) and CO_2 selectivity versus time-on-stream for the catalysts NCG, NCL, NCN and NCS and for the support CG during the partial oxidation of methane to syngas (T = 700 °C, P = 0.1 MPa, 36600 mL_N h^{-1} g^{-1}, CH_4/O_2 = 2).

Please cite this article in press as: Alvarez-Galvan C, et al., Cermets Ni/($Ce_{0.9}Ln_{0.1}O_{1.95}$) (Ln = Gd, La, Nd and Sm) prepared by solution combustion method as catalysts for hydrogen production by partial oxidation of methane, International Journal of Hydrogen Energy (2018), https://doi.org/10.1016/j.ijhydene.2018.04.025

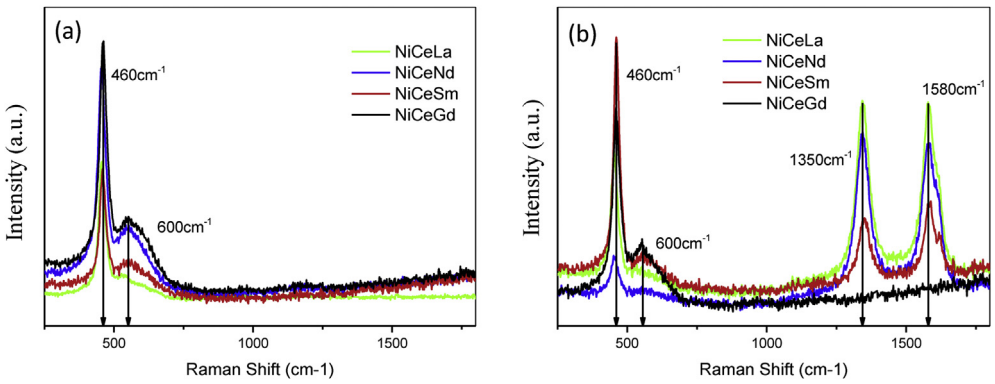

Fig. 10 – Raman spectra of the catalysts NCG, NCL, NCN and NCS (a) fresh (b) after reaction.

(corresponding to disordered and graphitic species, respectively) has been divided by the intensity of the band at 460 cm^{-1}, related to CeO_2. The values point out that gadolinium-doped catalyst does not present carbon deposits and samarium-doped catalyst presents a low amount of carbon deposits. On the contrary, the samples doped with lanthanum and neodymium show a larger amount of carbon.

Structure-activity correlations

The characterization of the catalysts by XRD proved the formation of fluorite-type oxides with high crystallinity and the absence of phases of single oxides of La, Gd, Nd or Sm. The color and magnetic properties of the catalysts point out the formation of metallic nickel, which is confirmed by XRD for higher Ni molar contents. This would indicate that the conditions used in this SCS method allows obtaining in a single step a material (cermet) composed by metallic nickel nanoparticles supported on the corresponding mixed oxide. The as-prepared catalysts present high macroporosity (revealed by SEM and Hg porosimetry) that increases the specific surface area of nickel and support (catalyst surface area per unit mass of catalyst). This fact is relevant since produces higher mass-specific activity and favors heat and mass transfer.

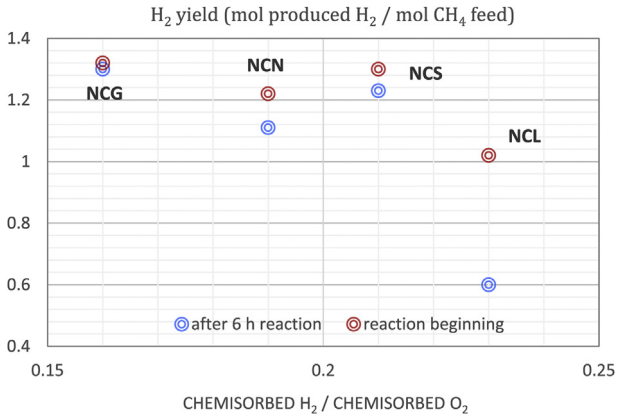

Fig. 11 – H_2 yield versus chemisorbed H_2 (catalysts)/ chemisorbed O_2 (supports) (mol/mol) for the catalysts NCG, NCL, NCN and NCS.

Fig. 11 depicts the hydrogen yields at the reaction beginning and after 6 h of reaction as a function of chemisorbed H_2/chemisorbed O_2 ratio. A significant trend is identified for both correlations. The highest hydrogen yields are found with a greater chemisorbed H_2/chemisorbed O_2 ratio, which points out the cooperative effect of both nickel and lanthanide-doped ceria. It would be necessary to develop some other catalysts compositions, in order to obtain higher ratios, greater than the highest value found for the catalysts studied in this work (around 0.16), to confirm the role of this parameter on the reactivity for POM to syngas and to figure out if there is an optimum ratio.

Thus, and in accordance with literature [28], the performance of the catalyst is influenced by a proper balance between OSC of the support and Ni dispersion. The higher OSC of the catalyst helped to remove the carbon deposits from the metal-support interface; thereby, a low metal dispersion, for a same OSC of the support, would decrease the metal-support interfacial area and hence the effectiveness for carbon removal.

The better catalytic efficiency of the catalyst doped with Gd, very active and stable, with no formation of carbon deposits, is related to a certain nickel surface area/surface oxygen vacancies proportion [19,38] and a high porosity, which favours mass and heat transfer. On the contrary, the worst catalytic performance is found for the lanthanum-doped catalyst, which shows a pronounced deactivation with time on stream, together with an increase in the selectivity to methane combustion and high carbon formation. This catalyst presents a Ni dispersion/chemisorbed oxygen ratio far from the corresponding to the catalyst with the best catalytic performance (NCG) and a lower porosity, which would have an influence on mass and heat transfer, favoring carbon formation by methane dehydrogenation. The lower selectivity to hydrogen shown for NCL catalyst that decreases with reaction time, points out that (i) the metallic nickel phase is becoming oxidized (as widely reported, nickel oxide is active for methane combustion) and/or that (ii) the proportion of surface metallic nickel or surface Ce–La mixed oxide decreases by carbon deposition [2]. However, considering that it is not possible to distinguish by XPS the surface proportion of carbon from carbonates and from carbon deposits, with the experimental data presented in this research work, both options should be left open.

Please cite this article in press as: Alvarez-Galvan C, et al., Cermets Ni/($Ce_{0.9}Ln_{0.1}O_{1.95}$) (Ln = Gd, La, Nd and Sm) prepared by solution combustion method as catalysts for hydrogen production by partial oxidation of methane, International Journal of Hydrogen Energy (2018), https://doi.org/10.1016/j.ijhydene.2018.04.025

Conclusions

The results obtained in this study show that the catalysts, prepared by SCS method, consist of composite materials based on metallic nickel nanoparticles supported on highly crystalline Ce-lanthanide mixed oxides, $(Ni)_{0.1}(Ce_{0.9}Ln_{0.1}O_{1.95})_{0.9}$ (Ln = Gd, La, Nd and Sm). This is an important advantage compared to conventionally impregnated catalysts, since a reduction step, prior to the reaction, is not required. On the other hand, the catalysts present high porosity, which increases active phase dispersion and, subsequently, the activity per unit mass of catalyst. The redox pair of ceria (Ce^{4+}/Ce^{3+}) and the doping of ceria with lanthanides induce the formation of oxygen vacancies and hence a better oxygen mobility. Both factors have a role in oxygen adsorption, in reactivity and in effectively removing carbonaceous deposits. The catalysts present high macroporosity, high crystallinity, high oxygen storage capacity, high thermal resistance and small particle size. The catalysts show high activity per mass unit for hydrogen production by partial oxidation of methane, which is mainly related to their high porosity and nickel dispersion. A trend between H_2 yield and Ni dispersion/OSC has been found, pointing to a cooperative and synergic effect between nickel and the doped-ceria support for this reaction. According to the obtained results, the best catalytic behavior is identified for the sample doped with gadolinium, for which no carbon formation is observed. Structure-activity correlations suggest that the ratio between Ni dispersion and the oxygen chemisorption capacity of the doped-ceria support plays a crucial role in the reactivity for POM to syngas, which also has an effect on the surface proportion of metallic nickel. On the contrary, the catalyst doped with lanthanum shows the lowest catalytic performance. This catalyst produces lower methane conversion, lower hydrogen yield and a pronounced deactivation with reaction time. This is explained by its lower porosity and high carbon formation favoured by a nickel surface area/chemisorbed O_2 ratio far from the optimum interval.

Acknowledgments

This work was supported by CSIC (Spain) through the grant 201680I045. The authors gratefully acknowledge Concepción Diaz Guerri for XRD analyses, Rosa Folgado Martínez for N_2 adsorption-desorption isotherms and Nieves Lopez Cortés for Hg porosimetry analyses.

REFERENCES

[1] Mokrani T, Scurrell M. Gas conversion to liquid fuels and chemicals: the methanol route-catalysis and processes development. Catal Rev Sci Eng 2009;51:1–145.
[2] York APE, Xiao TC, Green MLH. Brief overview of the partial oxidation of methane to synthesis gas. Top Catal 2003;22:345–58.
[3] Zhao S, Gorte RJ. A comparison of ceria and Sm-doped ceria for hydrocarbon oxidation reactions. Appl Catal A Gen 2004;277:129–36.
[4] Zhu T, Flytzani Stephanopoulos M. Catalytic partial oxidation of methane to synthesis gas over Ni–CeO_2. Appl Catal A Gen 2001;208:403–17.
[5] Pantu P, Gavalas G. Methane partial oxidation on Pt/CeO_2 and Pt/Al_2O_3 catalysts. Appl Catal A Gen 2002;223:253–60.
[6] Green MLH, Tsang SC, Claridge JB. Recent advances in the conversion of methane to synthesis gas. Catal Today 1995;23:3–15.
[7] Xie J, Sun X, Barrett L, Walker B, Karote D, Langemeier J, et al. Autothermal reforming and partial oxidation of n-hexadecane via Pt/Ni bimetallic catalysts on ceria-based supports. Int J Hydrogen Energy 2015;40:8510–21.
[8] Pantaleo G, La Parola V, Deganello F, Singha RK, Bal R, Venezia AM. Ni/CeO_2 catalysts for methane partial oxidation: synthesis driven structural and catalytic effects. Appl Catal B Environ 2016;189:233–41.
[9] Peymani M, Alavi S, Rezaei M. Preparation of highly active and stable nanostructured Ni/CeO_2 catalysts for syngas production by partial oxidation of methane. Int J Hydrogen Energy 2016;41:6316–25.
[10] Larimi AS, Alavi SM. Ceria-Zirconia supported Ni catalysts for partial oxidation of methane to synthesis gas. Fuel 2012;102:366–71.
[11] Dajiang M, Yaoqiang C, Junbo Z, Zhenling W, Di M. Catalytic partial oxidation of methane over Ni/CeO_2-ZrO_2-Al_2O_3. J Rare Earths 2007;25:311–5.
[12] Xu S, Wang XL. Highly active and coking resistant Ni/CeO_2–ZrO_2 catalyst for partial oxidation of methane. Fuel 2005;84:563–7.
[13] Pengpanich S, Meeyoo V, Rirksomboon T. Methane partial oxidation over Ni/CeO_2–ZrO_2 mixed oxide solid solution catalysts. Catal Today 2004;93–5:95–105.
[14] Dong W-S, Jun K-W, Roh H-S, Liu Z-W, Park S-E. Comparative study on partial oxidation of methane over Ni/ZrO_2, Ni/CeO_2 and Ni/Ce–ZrO_2 catalysts. Catal Lett 2002;78:215–22.
[15] Zhu QZZ, Deng Y. Advances in the partial oxidation of methane to synthesis gas. J Nat Gas Chem 2004;13:191–203.
[16] Prasad DH, Prasad DH, Jung HY, Kim BK. Single step synthesis of nano-sized NiO–Ce0.75Zr0.25O_2 composite powders by glycine nitrate process. Mater Lett 2008;62:587–90.
[17] Specchia S, Galletti C, Specchia V. Solution Combustion Synthesis as intriguing technique to quickly produce performing catalysts for specific applications. Stud Surf Sci Catal 2010;175:59–67.
[18] Pino L, Vita A, Cipiti F, Lagana M, Recupero V, Cipitì F, et al. Hydrogen production by methane tri-reforming process over Ni–ceria catalysts: effect of La-doping. Appl Catal B Environ 2011;104:64–73.
[19] Salazar Villalpando M, Reyes B. Hydrogen production over Ni/ceria-supported catalysts by partial oxidation of methane. Int J Hydrogen Energy 2009;34:9723–9.
[20] Alvarez-Galvan MDO MC, Alonso-Alonso JA, Troncoso Aguilera L, Cascos Jimenez V, Campos-Martin JM, García Fierro JL, et al. Patent application. 2017. ES1641.1265 BIS (application number: P201730807).
[21] Rietveld HM. A profile refinement method for nuclear and magnetic structures. J Appl Crystallogr 1969;2:65–71.
[22] Rodriguez Carvajal J. Recent advances in magnetic structure determination by neutron powder diffraction. Phys B Condens Matter 1993;192:55–69.
[23] Mattos LV, Noronha FB. Hydrogen production for fuel cell applications by ethanol partial oxidation on Pt/CeO2 catalysts: the effect of the reaction conditions and reaction mechanism. J Catal 2005;233:453–63.
[24] Burbano M, Nadin S, Marrocchelli D, Salanne M, Watson GW. Ceria co-doping: synergistic or average effect? Phys Chem Chem Phys 2014;16:8320–31.

Please cite this article in press as: Alvarez-Galvan C, et al., Cermets Ni/($Ce_{0.9}Ln_{0.1}O_{1.95}$) (Ln = Gd, La, Nd and Sm) prepared by solution combustion method as catalysts for hydrogen production by partial oxidation of methane, International Journal of Hydrogen Energy (2018), https://doi.org/10.1016/j.ijhydene.2018.04.025

[25] Kullgren J, Hermansson K, Broqvist P. Supercharged low-temperature oxygen storage capacity of ceria at the nanoscale. J Phys Chem Lett 2013;4:604–8.
[26] Villoria JA, Alvarez-Galvan MC, Al-Zahrani SM, Palmisano P, Specchia S, Alvarez Galvan MC, et al. Oxidative reforming of diesel fuel over LaCoO3 perovskite derived catalysts: influence of perovskite synthesis method on catalyst properties and performance. Appl Catal B Environ 2011;105:276–88.
[27] Passos FB, de Oliveira ER, Mattos LV, Noronha FB. Partial oxidation of methane to synthesis gas on Pt/CexZr1−xO2 catalysts: the effect of the support reducibility and of the metal dispersion on the stability of the catalysts. Catal Today 2005;101:23–30.
[28] Nahar G, Dupont V. Hydrogen production from simple alkanes and oxygenated hydrocarbons over ceria–zirconia supported catalysts: Review. Renew Sustain Energy Rev 2014;32:777–96.
[29] Alvarez-Galvan MC, Navarro RM, Rosa R, Briceno Y, Alvarez FG, Alvarezgalvan M. Performance of La,Ce-modified alumina-supported Pt and Ni catalysts for the oxidative reforming of diesel hydrocarbons. Int J Hydrogen Energy 2008;33:652–63.
[30] Luisetto I, Tuti S, Battocchio C, Lo Mastro S, Sodo A. Ni/CeO_2–Al_2O_3 catalysts for the dry reforming of methane: the effect of CeAlO3 content and nickel crystallite size on catalytic activity and coke resistance. Appl Catal A Gen 2015;500:12–22.
[31] Frolova YV, Sadykov V, Moroz EM, Alikina G, Lukashevich A, Muzykantov V, et al. Mobility and reactivity of the lattice oxygen of Pr-doped ceria promoted with Pt. React Kinet Catal Lett 2005;86:21–8.
[32] Shyu JZ, Otto K. Characterization of Pt/gamma-alumina catalysts containing ceria. J Catal 1989;115:16–23.
[33] Alvarez Galvan MC, Rosa F, Fierro JLG, Navarro RM. Hydrogen production by oxidative reforming of hexadecane over Ni and Pt catalysts supported on Ce/La-doped Al_2O_3. Appl Catal Gen 2006;297:60–72.
[34] Estrade Szwarckopf H. XPS photoemission in carbonaceous materials: a "defect" peak beside the graphitic asymmetric peak. Carbon 2004;42:1713–21.
[35] Li Y, Zhang C, Liu Y, Chen G, Tang S, Zhang R, et al. Study of X-ray photoelectron spectroscopy on coke deposited on Ni/HZSM-5 in bio-oil hydrodeoxygenation. React Kinet Mech Catal 2016;117:801–13.
[36] Reddy B, Rao K, Bharali P. Copper promoted cobalt and nickel catalysts supported on Ceria–Alumina mixed oxide: structural characterization and CO oxidation activity. Ind Eng Chem Res 2009;48:8478–86.
[37] Reddy B, Khan A, Lakshmanan P, Aouine M, Loridant S, Volta J-C. Structural characterization of nanosized CeO_2-SiO_2, CeO_2-TiO_2, and CeO_2-ZrO_2 catalysts by XRD, Raman, and HREM techniques. J Phys Chem B 2005;109:3355–63.
[38] Pereniguez R, Caballero A, Holgado J, Gonzalez Delacruz V, Ternero F, Pereñíguez R. Study of nanostructured Ni/CeO2 catalysts prepared by combustion synthesis in dry reforming of methane. Appl Catal A Gen 2010;384:1–9.

Please cite this article in press as: Alvarez-Galvan C, et al., Cermets Ni/($Ce_{0.9}Ln_{0.1}O_{1.95}$) (Ln = Gd, La, Nd and Sm) prepared by solution combustion method as catalysts for hydrogen production by partial oxidation of methane, International Journal of Hydrogen Energy (2018), https://doi.org/10.1016/j.ijhydene.2018.04.025